Metamaterials for optical Bragg accelerators

Adi Hanuka,[a] Elron Goldemberg, Almog Zilka, and Levi Schächter
Department of Electrical Engineering, Technion–Israel Institute of Technology, Haifa 32000, Israel

(Received 5 December 2017; accepted 22 February 2018; published online 5 March 2018)

We present a systematic study of the advantages of using optical artificial materials in designing periodic structures for laser-driven accelerators. As a case study, we investigate the electromagnetic properties of a Bragg waveguide, with its alternating layers being composed of artificial materials. The layers can be optimized to maximize the structure's properties. We show that when the structure's eigenmode interacts with free electrons, the maximum efficiency is nearly four times higher than in configurations that rely on natural materials. As a result, accelerators and radiation sources may be miniaturized significantly. *Published by AIP Publishing.* https://doi.org/10.1063/1.5018251

Throughout the years, several *periodic* structures have been proposed for laser-driven acceleration of charged particles, mostly consisting of dielectric materials: Lin's 2D photonic bandgap (PBG) structure,[1] Mizrahi's Bragg-structure,[2] Cowan's 3D PBG,[3] and the wood-pile configuration.[4] An extended review of the various structures considered was recently published.[5] Common to all such dielectric structures is relatively low efficiency (<10%) of energy conversion from free electrons to the structure's eigenmode and vice-versa.

Although in the optical regime, most such structures are composed of dielectric materials, artificial materials could also be considered. Artificial materials for optical frequencies have raised strong interest in recent years;[6] photonic bandgap materials,[7] photonic crystal fibers, negative permeability, permittivity,[8] and negative refractive index materials[9] are all being investigated, within a variety of geometries. The fabrication of such metamaterials is challenging,[10] but the technology continues to advance; therefore, it is important to investigate frontiers. Recently, a comprehensive study on the road-map of optical metamaterials has been published.[11] Among the applications for metamaterials are optical sensors detecting chemical or biological species,[12] optical cloaking,[13] imaging,[14] laser-driven accelerators,[15] and plasmonics and nanophotonics.[16]

Considering low efficiency of current periodic structures, coupled with recent advancements in optical artificial materials, in this study, we explore applying the latter in order to enhance the electromagnetic properties (efficiency and group velocity) of periodic structures. We systematically explore a variety of artificial materials for multi-layer Bragg planar waveguides and show that by meticulously selecting the materials, an efficiency of 35% is viable. The concept could be generalized for different configurations, e.g., cylindrical waveguide, grating, or honey-comb structure, and presents opportunities for designing new optical functionalities in integrated optics.

Due to the quasi-analytical character of its analysis, we adopt a planar Bragg waveguide[2] for the examples brought subsequently. We consider the former to consist of a series of alternating layers of two artificial materials: the first material (subscript I) has dielectric and permeable properties denoted by ε_{I} and μ_{I}, respectively, and the second material (subscript II) is characterized by $\varepsilon_{\mathrm{II}}$ and μ_{II}. Between the two sides of the Bragg layers, there is a vacuum clearance of width $2D_{\mathrm{int}}$, as shown in Fig. 1.

In this configuration, we assume that a wave propagates in the z-direction (denoted as longitudinal) with a phase velocity equaling the speed of light in *vacuum* (c); no variations are assumed in the y-direction; the Bragg structure is quasi-periodic in the x-direction (denoted as transverse). Note that for the results presented subsequently, we truncated the structure after 30 layers[15] since, in practice, the electric field decays to negligible values. Furthermore, we assume a single TM_{01} mode consisting of three components (E_x, E_z, and H_y).

The transverse wave vector of the ν-th layer is $k_{x,\nu} = \omega\sqrt{\mu_\nu\varepsilon_\nu - 1}/c$, and its transverse impedance is $Z_\nu = \eta_0\sqrt{\mu_\nu\varepsilon_\nu - 1}/\varepsilon_\nu$, where η_0 is the wave impedance in vacuum. The boundary conditions are formulated in a matrix form,[15] including the first matching layer ($\nu = 1$) which does not satisfy the Bragg condition but is essential for matching between the mode in vacuum to the mode in the remaining periodic Bragg layers.

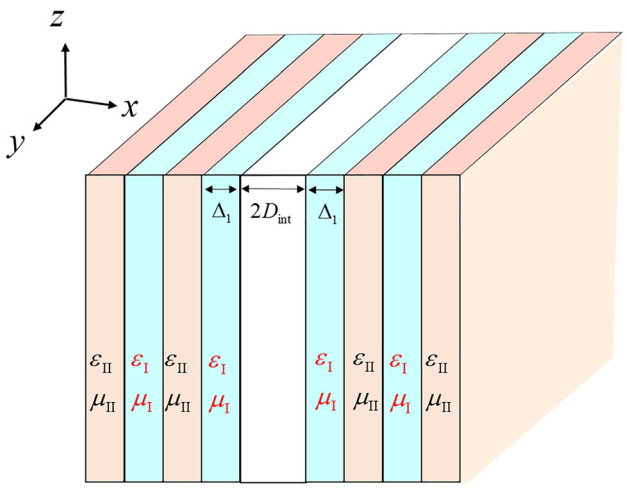

FIG. 1. Schematics of the envisaged configuration: planar Bragg waveguide with a vacuum clearance of $2D_{\mathrm{int}}$ and alternating layers of two artificial materials. The first layer (its width being Δ_1) is composed of an artificial material with dielectric and permeable properties of ε_{I} and μ_{I}, respectively.

[a]Electronic mail: Adiha@tx.technion.ac.il

In the design process, we distinguish between two cases: if $Z_1 > Z_2$, the longitudinal electric field vanishes[17] in the interface of the first and second layers, i.e., $E_z(x = D_{\text{int}} + \Delta_1) = 0$; it is therefore equivalent to a single layer case with a perfect electric conductor wall. In contrast, if $Z_1 < Z_2$, the magnetic field vanishes[17] in the interface of the first and second layers, i.e., $\partial E_z(x = D_{\text{int}} + \Delta_1)/\partial x = 0$; it is therefore equivalent to a single layer case with a perfect magnetic conductor wall. In what follows, we refer to the first case as the *electric* case and to the second as the *magnetic* case.

Before we proceed, we wish to emphasize a few assumptions that are at the foundations of this study: (i) we assume that the quality factor of the structure is large enough such that the field decay associated with loss (ohm or radiation) may be ignored but is sufficiently low to facilitate bandwidth which enables the propagation of the laser pulse. The effect of the loss in the artificial material and its compensation is configuration-dependent and is beyond the scope of this study. (ii) It is assumed that the optical artificial material is homogeneous and isotropic, namely, the spatial scale of the metamaterial's fine-scale features is presumably very small as compared to the wavelength in the material. (iii) At the practical level, one should consider laser pulses below the damage threshold fluence of the artificial material, which generally depends on the following: laser pulse duration, repetition rate, structure's geometry, surface polish, and defects.[18,19]

Efficiency is an important characteristic of the energy coupling between a wave propagating in a structure and free electrons. Maximizing this quantity might be crucial for some applications. For example, the efficiency of a laser-driven accelerator structure is a measure for the increase in the kinetic energy of a particle beam relative to an electromagnetic energy.

For the sake of formulating the *maximum* acceleration efficiency, we assume that an electromagnetic wave (wavelength $\lambda = 2\,\mu$m) co-propagates with a particle bunch. Since the former travels at the group velocity (v_{gr}) whereas the latter travels virtually at the speed of light in vacuum, a Cherenkov radiation is emitted, acting as a decelerating wake-field. The latter is proportional to the charge in the bunch, and the proportionality factor is denoted by κ.[20] The maximum acceleration efficiency[21] (η_{max}) is determined by the projection of the fundamental mode of the wake (κ_1) on the total decelerating wake ($\kappa = 1/4\varepsilon_0 D_{\text{int}}$ as in Ref. 22), i.e.,

$$\eta_{\text{max}} \equiv \frac{\kappa_1}{\kappa} = \frac{Z_{\text{int}} v_{\text{gr}}}{4\lambda^2 \left(1 - \frac{v_{\text{gr}}}{c}\right)\kappa}. \tag{1}$$

By virtue of linearity of Maxwell equations, the interaction impedance ($Z_{\text{int}} \equiv E_0^2 \lambda^2 / P$) is a measure of the longitudinal electric field experienced by the particles (E_0) given the total amount of power injected into the system (P). The interaction impedance decreases monotonically for the wider vacuum channel. For example, for the electric case of the pure dielectric structure (presented in solid green in Fig. 2), Ref. 2 shows that $Z_{\text{int}}/\eta_0\lambda = 1.12 - 3.56(D_{\text{int}}/\lambda) + 4.25(D_{\text{int}}/\lambda)^2 - 1.82(D_{\text{int}}/\lambda)^3$. In the design process, our experience indicates that the interaction impedance has a larger impact on maximizing the efficiency relative to that of the group velocity. The latter increases whereas the former decreases as a function of D_{int}. These opposite trends between Z_{int} and v_{gr} result in an optimum point for the maximum efficiency. Note that Eq. (1) is independent of the wavelength.

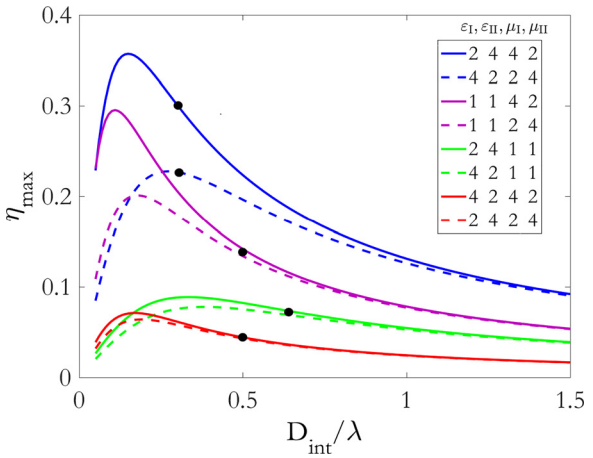

FIG. 2. Maximum efficiency as a function of half vacuum clearance for several combinations of dielectric and permeable materials. The variety of materials is organized in the following order ε_{I}, ε_{II}, μ_{I}, and μ_{II}, with a distinction between the electric (solid) and magnetic (dashed) cases. The black dots indicate the maximum D_{int} whereby a single mode propagation is ensured.

In what follows, we present the maximum efficiency and group velocity for four types of structures: pure permeable, pure dielectric, and two types of hybrid structures. The "hybrid I" structure contains artificial materials wherein $\varepsilon_{\text{I}} = \mu_{\text{I}}, \varepsilon_{\text{II}} = \mu_{\text{II}}$ and the "hybrid II" structure has $\varepsilon_{\text{I}} = \mu_{\text{II}}, \varepsilon_{\text{II}} = \mu_{\text{I}}$. For each structure type, we explore both the electric and magnetic cases. All four types of structures, consisting of 30 layers each, are summarized in Table I along with their transverse impedance for the electric case.

Figure 2 shows the maximum efficiency as a function of half vacuum clearance width, for four pairs of curves; each pair presents the electric (solid) and magnetic (dashed) cases for the same two materials (in reverse order). The variety of materials shown in the figure legend is organized in the following order: ε_{I}, ε_{II}, μ_{I}, μ_{II}, where ε and μ are the dielectric and permeable properties respectively, and the subscripts I or II refer to the odd or even layers. The black dots indicate the maximum D_{int} for each case wherein a *single* mode propagates.

It is important to make two observations: (i) for all curves, there is an optimum value of maximum efficiency which occurs for different values of vacuum clearance and (ii) for each structure type, the magnetic and electric cases consolidate as the vacuum clearance widens ($D_{\text{int}} > 0.5\lambda$). Below, we explore the features of each curve.

TABLE I. Summary of the four envisaged structures. The transverse impedances are presented for the electric case ($Z_1 > Z_2$) and are reversed for the magnetic case.

Structure type	Materials	Z_1 (Ω)	Z_2 (Ω)
Pure dielectric (green)	$\mu_{\text{I}} = 1, \mu_{\text{II}} = 1$	188	163
Pure permeable (purple)	$\varepsilon_{\text{I}} = 1, \varepsilon_{\text{II}} = 1$	653	377
Hybrid I (red)	$\varepsilon_{\text{I}} = \mu_{\text{I}}, \varepsilon_{\text{II}} = \mu_{\text{II}}$	365	326
Hybrid II (blue)	$\varepsilon_{\text{I}} = \mu_{\text{II}}, \varepsilon_{\text{II}} = \mu_{\text{I}}$	499	249

The *pure dielectric* structure ($\mu_I = \mu_{II} = 1$) is presented in green, where $Z_1 = 188\ \Omega$ and $Z_2 = 163\ \Omega$ for the electric case (solid) and vice versa for the magnetic case (dashed). The maximum efficiency of the electric case is nearly the same as compared with the magnetic case for small vacuum clearance, and its optimum value is smaller than 10%.

The *pure permeable* structure ($\varepsilon_I = \varepsilon_{II} = 1$) is presented in purple, where $Z_1 = 653\ \Omega$ and $Z_2 = 377\ \Omega$ for the electric case and vice versa for the magnetic case. The maximum efficiency of the electric case is higher than the corresponding value of the magnetic case for small vacuum clearance ($D_{int} < 0.5\lambda$), and in its optimum value, the maximum efficiency is 1.5 times higher in the electric case.

The *hybrid I* structure, presented in red, has $\varepsilon_I = \mu_I$ and $\varepsilon_{II} = \mu_{II}$, where $Z_1 = 365\ \Omega$ and $Z_2 = 326\ \Omega$ for the electric case and vice versa for the magnetic case; the difference between the two cases is negligible. Moreover, this structure presents the lowest maximum efficiency ($\eta_{max} < 7\%$).

The *hybrid II* structure, presented in blue, has $\varepsilon_I = \mu_{II}$ and $\varepsilon_{II} = \mu_I$, where $Z_1 = 499\ \Omega$ and $Z_2 = 249\ \Omega$ for the electric case and vice versa for the magnetic case; this structure presents the highest difference between the two cases for small vacuum clearance and the highest maximum efficiency ($\eta_{max} \sim 35\%$), occurring in the electric case.

When comparing all four structures, it is evident that the optimum value of efficiency increases as the contrast between the transverse impedances of adjacent layers (Z_1 and Z_2) increases. With this understanding in mind and the fact that the hybrid II structure presents the highest efficiency for both electric and magnetic cases separately, we further investigate the effect of the materials' combination on the maximum efficiency for the hybrid II structure. Specifically, we explore whether it is possible to further increase the efficiency.

Figure 3 plots the maximum efficiency of the hybrid II structure ($\varepsilon_I = \mu_{II}$ and $\varepsilon_{II} = \mu_I$) for $D_{int} = 0.3\lambda$ and various combinations of artificial materials. The area above the bold white line ($Z_1 = Z_2$) represents the electric case. Evidently, the maximum efficiency is maximized in the upper left corner, which indeed corresponds to the electric case. The highest value ($\eta_{max} \simeq 0.6$) occurs for cases where ε_{II} and μ_I are

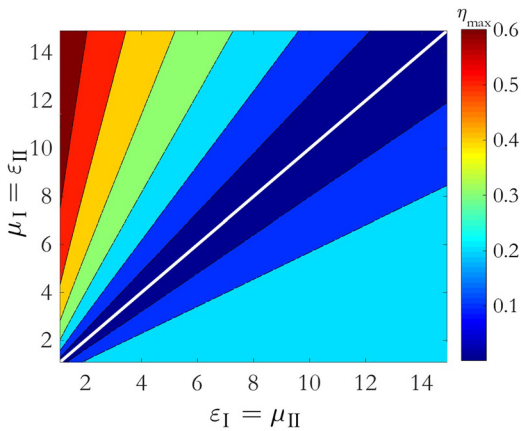

FIG. 3. Maximum efficiency for $D_{int} = 0.3\lambda$ and various combinations of dielectric and permeable materials for the hybrid II structure. The bold white line represents $Z_1 = Z_2$; the area above it corresponds to the electric case, which maintains higher efficiency than the magnetic case.

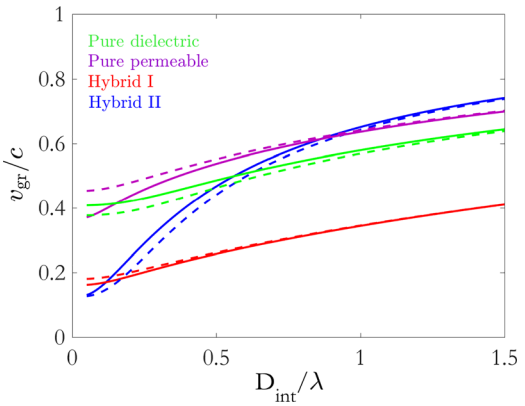

FIG. 4. Group velocity as a function of half vacuum clearance is shown in Fig. 4 for the same variety of materials as in the Fig. 2 legend.

significantly higher than ε_I and μ_{II}. Moreover, the efficiency vanishes on the diagonal line, in which $\varepsilon_I = \varepsilon_{II} = \mu_I = \mu_{II}$, since no confinement can be ensured.

Finally, the group velocity as a function of half vacuum clearance is shown in Fig. 4 for the same variety of materials as in the Fig. 2 legend. Evidently, the group velocity for the electric and magnetic cases, for each type of structure, is nearly the same. Moreover, the hybrid II structure (blue), which presented the highest efficiency, has the widest range of group velocity and thus highly tunable.

In conclusion, we demonstrated the advantages of using optical artificial materials in periodic structures, with Bragg as a case study. In particular, the efficiency is optimized for a hybrid structure with a combination of artificial materials wherein $\varepsilon_I = \mu_{II}$ and $\varepsilon_{II} = \mu_I$. For such a hybrid structure, designing the composition of the layers so that the transverse impedance of the first layer is greater than that of the second layer ($Z_1 > Z_2$) yields the optimal efficiency, its maximum being nearly four times higher than previous studies have shown for pure dielectric structures.

The case of $Z_1 > Z_2$, referred to as the electric case, presents higher efficiency than the magnetic case ($Z_1 < Z_2$). This is evident for all material combinations, such as pure permeable, pure dielectric, or hybrid structures wherein $\varepsilon_I = \mu_I$ and $\varepsilon_{II} = \mu_{II}$. The electric case outperforms the magnetic case because the energy stored in the vacuum channel is higher as compared with the energy stored in the material. This study opens up opportunities for enabling highly tunable periodic structures for various applications, where efficiency and group velocity are a critical figure of merit.

This study was supported by Israel Science Foundation and Rothschild Caesarea Foundation.

[1]X. Lin, "Photonic band gap fiber accelerator," Phys. Rev. Spec. Top. - Accel. Beams **4**, 051301 (2001).
[2]A. Mizrahi and L. Schächter, "Optical Bragg accelerators," Phys. Rev. E **70**, 016505 (2004).
[3]B. M. Cowan, "Photonic crystal laser-driven accelerator structures," Ph.D. thesis (Stanford University, 2007).
[4]Z. Wu, R. J. England, C.-K. Ng, B. Cowan, C. McGuinness, C. Lee, M. Qi, and S. Tantawi, "Coupling power into accelerating mode of a three-dimensional silicon woodpile photonic band-gap waveguide," Phys. Rev. Spec. Top. - Accel. Beams **17**, 081301 (2014).
[5]R. J. England *et al.*, "Dielectric laser accelerators," Rev. Mod. Phys. **86**, 1337–1389 (2014).

[6]D. Lippens, "Overview of microwave and optical metamaterial technologies," in *Metamaterials and Wave Control*, edited by E. Lheurette (ISTE Ltd., 2013).
[7]M. Iwanaga, "Photonic metamaterials: A new class of materials for manipulating light waves," Sci. Technol. Adv. Mater. **13**, 053002 (2012).
[8]A. Boltasseva and V. M. Shalaev, "Fabrication of optical negative-index metamaterials: Recent advances and outlook," Metamaterials **2**, 1–17 (2008).
[9]D. R. Smith, J. B. Pendry, and M. C. K. Wiltshire, "Metamaterials and negative refractive index," Science **305**, 788–792 (2004).
[10]G. Yoon, I. Kim, and J. Rho, "Challenges in fabrication towards realization of practical metamaterials," Microelectron. Eng. **163**, 7–20 (2016).
[11]A. M. Urbas, Z. Jacob, L. D. Negro, N. Engheta, A. D. Boardman, P. Egan, A. B. Khanikaev, V. Menon, M. Ferrera, N. Kinsey, C. DeVault, J. Kim, V. Shalaev, A. Boltasseva, J. Valentine, C. Pfeiffer, A. Grbic, E. Narimanov, L. Zhu, S. Fan, A. Alù, E. Poutrina, N. M. Litchinitser, M. A. Noginov, K. F. MacDonald, E. Plum, X. Liu, P. F. Nealey, C. R. Kagan, C. B. Murray, D. A. Pawlak, I. I. Smolyaninov, V. N. Smolyaninova, and D. Chanda, "Roadmap on optical metamaterials," J. Opt. **18**, 093005 (2016).
[12]Z. Jakšić, "Optical metamaterials as the platform for a novel generation of ultrasensitive chemical or biological sensors," in *Metamaterials: Classes, Properties and Applications* (Nova Science Publishers, 2010), pp. 1–42.
[13]W. Cai, U. Chettiar, A. Kildishev, and V. Shalaev, "Optical cloaking with metamaterials," Nat. Photonics **1**, 224 (2007).
[14]G. Shvets, S. Trendafilov, J. B. Pendry, and A. Sarychev, "Guiding, focusing, and sensing on the subwavelength scale using metallic wire arrays," Phys. Rev. Lett. **99**, 053903 (2007).
[15]A. Hanuka, E. Goldemberg, A. Zilka, and L. Schächter, "Artificial materials for structure-based laser acceleration," in *Proceedings of AAC16* (2017), p. 060008.
[16]N. C. Lindquist, P. Nagpal, K. M. McPeak, D. J. Norris, and S.-H. Oh, "Engineering metallic nanostructures for plasmonics and nanophotonics," Rep. Prog. Phys. **75**, 036501 (2012).
[17]A. Mizrahi and L. Schächter, "Bragg reflection waveguides with a matching layer," Opt. Express **12**, 3156–3170 (2004).
[18]A. Hanuka, L. Schächter, K. P. Wootton, Z. Wu, K. Soong, I. V. Makasyuk, and R. J. England, "Cumulative damage of ultafast laser pulses," in *Proceedings of IPAC16* (2016), pp. 1–4.
[19]K. Soong, R. L. Byer, E. R. Colby, R. J. England, and E. A. Peralta, "Laser damage threshold measurements of optical materials for direct laser accelerators," AIP Conf. Proc. **1507**, 516 (2012).
[20]L. Schächter, R. L. Byer, and R. H. Siemann, "Wake field in dielectric acceleration structures," Phys. Rev. E **68**, 036502 (2003).
[21]K. Bane and G. Stupakov, "Impedance of a rectangular beam tube with small corrugations," Phys. Rev. Spec. Top. - Accel. Beams **6**, 024401 (2003).
[22]A. Hanuka and L. Schächter, "Bragg accelerator optimization," High Power Laser Sci. Eng. **2**, e24 (2014).